Accepted Manuscript

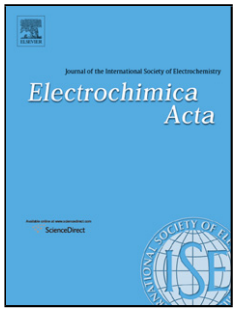

Title: Hybrid sol-gel coatings containing clay nanoparticles for corrosion protection of mild steel

Author: Ianina Santana Andrés Pepe Wido Schreiner Sergio Pellice Silvia Ceré

PII: S0013-4686(16)30241-9
DOI: http://dx.doi.org/doi:10.1016/j.electacta.2016.01.214
Reference: EA 26596

To appear in: *Electrochimica Acta*

Received date: 30-9-2015
Revised date: 26-1-2016
Accepted date: 29-1-2016

Please cite this article as: Ianina Santana, Andrés Pepe, Wido Schreiner, Sergio Pellice, Silvia Ceré, Hybrid sol-gel coatings containing clay nanoparticles for corrosion protection of mild steel, Electrochimica Acta http://dx.doi.org/10.1016/j.electacta.2016.01.214

Hybrid sol-gel coatings containing clay nanoparticles for corrosion protection of mild steel

Ianina Santana[1], Andrés Pepe[1], Wido Schreiner[2], Sergio Pellice[1], Silvia Ceré[1*]

[1]INTEMA, Universidad Nacional de Mar del Plata - CONICET, Juan B. Justo 4302, B7608FDQ. Mar del Plata, Argentina.

[2]LSI – LANSEN, Departamento de Física, UFPR. Curitiba, Brasil

*Corresponding author and ISE active member.
División Electroquímica y Corrosión, Facultad de Ingeniería, Universidad Nacional de Mar del Plata, INTEMA, CONICET
Juan B. Justo 4302 - B7608FDQ Mar del Plata – Argentina
e-mail: *smcere@fi.mdp.edu.ar*
Tel.: +54 223 481 6600 ext 244, Fax: +54 223 481 0046

Highlights

- Barrier properties of thin sol-gel coatings were improved with clay nanoparticles.
- Self-healing effect was achieved with addition of Ce(III) ions in sol-gel films.
- Clay nanoparticles and the cerium salt enhance corrosion protection of the mild steel.

Abstract

The development of a new environment-friendly anticorrosive coating for mild steel substrate is afforded in this work. The combined use of cerium, as a self-healing agent, and clay nanoparticles, as improvers of the barrier properties, was considered to the development of new anticorrosive sol-gel coatings. Nanostructured hybrid films were synthesized by the sol–

gel route from tetraethoxysilane (TEOS) and 3-glicidoxipropyl-trimetoxisilano (GPTMS) using laminar nanoclays (Laponite $Na^{+}_{0.7}[Si_8Mg_{5.5}Li_{0.3}H_4O_{24}]^{-}_{0.7}$) to improve mechanical and barrier properties, and $Ce(NO_3)_3 \bullet 6H_2O$ as a supplier of Ce(III) to provide an inhibiting effect in the event of coating failure. Carbon steel plates, AISI 1010, were used as substrates. Prior to the application of the coating, samples were treated with a phosphoric acid 2 % v/v in order to improve coating adherence.

In order to evaluate cerium effect, electrochemical behaviour of films containing Laponite and cerium salts (TGL-Ce) were compared with films containing only Laponite (TGL) by means of potentiodynamic polarization tests and electrochemical impedance spectroscopy (EIS) measurements using a 0.35 wt% NaCl solution. Microstructural characterization and surface analysis of substrates and sol-gel coatings were performed by optical microscopy and by XPS techniques. The use of nanoclays allowed to achieve a significant improvement of the anticorrosive behaviour of the cerium doped coating at the same time that enhances the physical integrity of the coatings under immersion tests.

Keywords: mild steel; cerium; corrosion; silanes.

1. Introduction

Since the adoption of new regulations towards protection of the environment, in the field of the industrial anticorrosive products, the use of chromate based coatings is highly limited, being, at the moment, only permitted for the aeronautical industry, were the high performance of the chromate conversion coatings (CCC) is, at the moment, the only that provides the necessary safety criteria. So, the development of new environment-friendly high performance anticorrosive coatings is a hot topic for the scientific researchers due to the increasing demand

from the industrial field. Is in this framework were the called self-healing coatings take wide importance thanks to their possibility of present a long-term anticorrosive protection with the use of safer compounds as the based on lanthanides elements like Ce and La [1,2].

The sol-gel science is a very promising alternative to allow us to reach a functional material coating that fulfills the high demands of the industrial field, as it is the high physicochemical and thermal stability and its possibility to incorporate almost any kind of functional additives as organic compounds and ionic salts [3,4]. Furthermore, sol-gel coatings are compatible with a variety of substrates and can be applied as very thin coatings. The development of a three-dimensional silica network as the main component of the coating structure can offer a well densified material with extremely good barrier properties [5,6,7,8,9]. For this reason, the research in the sol-gel field for anticorrosive coatings is worldwide extended. Nevertheless, the addition of ionic salts, behind conferring the desired functionality, usually carries to a detrimental of the barrier properties by its function as network modifiers. Then, to produce a Ce-functionalized self-healing coating, the use of multilayer coatings is a common strategy in order to reach both the barrier and self-healing properties. The barrier properties of sol-gel coatings can be substantially improved by controlling the crosslinking density of its structure or by incorporation of denser nanoparticles that, at the same time, work as mechanical reinforcement. Even so, the structural modification introduced by lanthanide compounds on the silica network leaves an open path to the water diffusion through the coating [10].

In the recent years, the development of new nanocomposites was highly explored by the use of nano-clays thanks to its highly availability and economical convenience. Those nanoparticles are highly employed as rheological modifiers in the industry of cosmetic and paints and, at the same time, their use as load for composite materials can improve both the mechanical and barrier properties[11,12,13]. However, the use of clay nanoparticles in the field of sol-gel thin coatings is an area that has not been extendedly analyzed[14,15,16]. The

synthesis of a sol with an appropriated load of well exfoliated clay nanoparticles, and its deposition as a coating by the dip-coating process, could carry to the development of a high performance sol-gel material. This combination of material and deposition process is able to produce a matrix were the clay particles remain perfectly aligned with the substrate increasing the diffusive pathway for the corrosion process and a direct diffusive pathway for the active Ce ions towards the presence of an occasional defect or damage in the coating to confer the desired self-healing property.

In this work, we present a novel strategy to provide a single-layer sol-gel coating with improved barrier and self-healing properties through the nano-structuring of its organic-inorganic hybrid matrix with the use of exfoliated synthetic nano-clays as potential prime coatings.

2. Experimental

2.1. Synthesis and deposition

Three different sols were synthesized in order to analyse the anticorrosive behaviour of cerium-doped coatings with a stratified laminar structure: an epoxy-silica hybrid sol (TG), a hybrid sol loaded with laminar nanoparticles (TGL) and a hybrid sol with laminar nanoparticles and cerium dopping (TGL-Ce). Hybrid sols were synthesized from the hydrolytic condensation of tetraethoxysilane (TEOS, Aldrich 99%) and glycidoxypropil-trimetoxysilane (GPTMS, Aldrich 98%) in acidic media using concentrated HNO_3 as catalyser. In order to incorporate the laminar nanoparticles in the precursor solution, hydrolysis of TGL sol was performed in presence of an aqueous suspension of a synthetic exfoliated clay nanoparticles (Laponite S482 ®, Rockwood Specialties, Inc.). $CeNO_3$ was used as supplier of cerium. In every case, TEOS/GPTMS molar ratio was kept to 60/40, Laponite was incorporated at a 0.5 wt % in respect to condensed silica and Ce(III) was added, from cerium nitrate, to attain a Ce/alkoxides molar ratio of 5/95.

Precursor sols were deposited by the dip coating process on AISI 1010 mild steel plates previously degreased and treated with phosphoric acid following a reported procedure [17][in order to improve the coating adhesion. After deposition, coated substrates were thermally treated at 120 ºC in air atmosphere during 2 hours. Figure 1 shows a schematic representation of the samples preparation.

2.2. Coatings Characterization

Morphology of the obtained coatings was analyzed through optical microscopy (Olympus, PMG3, Japan) in reflectance mode. Coating thickness was determined by mechanical profilometry (KLA Tecnor^{TM} D-100) on samples with a slope performed on the film by scratching immediately after deposition and before the thermal treatment. Every measurement was performed at five different points for every sample composition.

Coatings wettability was analyzed through contact angle measurements performed with a contact angle goniometer (Ramé Hart model 500) with DropImage Advanced Software. A 5 µL drop of bi-distilled water was applied on coatings at 20 ºC and a waiting time of 60 s was employed for every measurement. The process was repeated 4 times for every sample.

X-ray photoelectron spectroscopy (XPS) was performed with a TFA Physical Electronics Inc. spectrometer using non- and monochromatised Al K_α radiation (1486.6 eV) and a hemispherical analyzer. The monochromatised radiation used for high-resolution spectra yields a resolution of 0.6 eV, as measured on an Ag $3d_{5/2}$ peak. These spectra were used to differentiate the chemical environment of various species, whereas spectra obtained using the non-monochromatised variant were used for quantifying the chemical composition. A take-off angle (detection angle) of 45° with respect to the surface plane was used. The energy resolution was 0.5 eV. Survey scan spectra were recorded at a pass energy of 187.85 eV, and individual high-resolution spectra at a pass energy of 23.5 eV with an energy step of 0.1 eV.

During the analysis a small shift was observed which was compensated by neutraliser. The values of binding energies were then aligned to carbon peak C 1s at 285.0 eV. The XPS measurements were repeated at several spots on the sample surface; the results were found to be similar. Representative measurements are reported.

2.3. Electrochemical behavior

Corrosion resistance was evaluated by means of a potentiodynamic polarisation test and electrochemical impedance spectroscopy (EIS) measurements in 0.35 wt.% NaCl solution prepared from p.a. grade chemicals (Sigma-Aldrich) and bidistilled water (Millipore, 18.2 MΩ cm). All measurements were carried out at room temperature (20 ± 1 °C) using a typical three-electrode configuration, with a saturated calomel electrode (SCE, Radiometer Analytical, France) as the reference electrode, a platinum wire of convenient area as counter electrode and the material to be tested as the working electrode. The latter was placed at the bottom of the cell, exposing an area of 3.54 cm^2. Electrochemical impedance spectroscopy (EIS) was performed at sweeping frequencies from 50,000 to 0.01 Hz and modulating 10 mV (rms) around the corrosion potential (E_{corr}). EIS fitting was performed using Zview software [18]. Potentiodynamic polarisation curves were scanned from −0.7 V to 1 V at a rate of 2 mV/s. All potentials in this work are referred to the saturated calomel electrode (0.241 vs Standard hydrogen electrode, SHE).

3. Results and Discussion

Transparent and colorless sols were obtained after the hydrolytic condensation. The dip coating process carried out to homogeneous, smooth and cracks free coatings. Independently of composition, all coatings were around 2µm thickness. Table 1 presents the thicknesses of coatings after thermal densification process.

3.1. Coatings Characterization

Surface wettability of coatings, determined through the contact angle of water drops, showed the same behaviour for the three compositions analysed, presenting a rather hydrophilic characteristic, in every case, with contact angle values lower than 90 º. Table 2 display the results of contact angle measurements obtained at 20 ºC. Besides the known hydrophilic property of clays, its incorporation to the formulation of TGL coating does not produced a change, in respect to TG coating. The relatively small amount of the employed clay nanoparticles used to provide the stratified structure was not enough to introduce any change in the wettability of the coatings. The contact angle resulting for the films is adequate to provide wettability in the event of applying a top coat on this films acting as primer [19].

Despite that three kind of coatings present the same thickness and the same wettability degree, after immersion of the samples in 0.35 wt% NaCl water solution at room temperature during 24 h a clear difference was observed between samples with and without clay nanoparticles. Figure 2 shows the micrographs of mild steel samples with TG, TGL and TGL-Ce coatings after 24 h immersion. Although generally no change in transparency nor colour was observed after immersion, TG samples presented a slight trend to blistering that was not observed in clay nanoparticles containing samples, as TGL and TGL-Ce. Due to the high transparency and colourless of the hybrid sol-gel coatings, the scratched microstructure of the grinded substrates can be clearly observed.

The superficial composition of sol-gel coatings was also analysed before and after 24 h of immersion through XPS. Figure 3 shows the high resolution spectra for Si 2p and O 1s. Both before and after 24h immersion in 0.35 wt% NaCl water solution, silicon 2p spectra of all the samples, Figures 3 *a*) and *b*), present a single peak around 102.6 eV without evident shifts as result of the different compositions or immersion time. This band in Si 2p XPS

spectra is characteristic of silicon bonded to carbon and/or oxygen as in silicones or hybrid organic-inorganic sol-gel samples.[20,21,22]. Analysis of the oxygen 1s spectra of all the samples not exposed to immersion, Figure 3 *c*), presented a single peak near the 532.6 eV, which is related to the bonding of oxygen with silicon (Si-O-Si) present in silica and silicones [20,21,23] which is consistent with the observed in silicon spectra of the same samples. So, the results obtained for just coated samples allows to determine that those are physically integer and that neither the incorporation of clay nanoparticles nor cerium salt has any evident effect on the silicon and oxygen atomic neighbourhoods. After 24 h immersion in the aqueous solution, Figure 3 *b*), the single peak of O 1s for TGL-Ce sample remains technically unchanged, while the spectra for TGL and TG samples present significant differences in respect to their respective initial conditions. While the peak related to silicon oxide remains as the dominant one, the immersion of TGL sample carried to the evolution of a shoulder peak at 530 eV, which is characteristic of Fe_2O_3. This observation could be considered as an evidence of a partial exposition and oxidation of the mild steel substrate as a consequence of a kind of loosening of the integrity of the TGL coating. In the case of TG sample, the immersion in the aqueous solution during 24 h produced a more pronounced change in the O 1s spectra. The peak corresponding to the silicon oxide, at 532.6 eV, was completely overlapped and only a near single peak at 531.6 eV, attributed to iron hydroxide, was observed.

As it could be expected from the observed in O 1s spectra, the analysis of Fe $2p_{3/2}$ XPS spectra, Figure 4, presented the characteristic peak attributed to Fe(II) and Fe(III) oxides, at 711.3 eV, for both TGL and TGL-Ce samples [24]. In the case of TG sample, an evident contribution of the Fe metal peak, at 707.7 eV, is also observed, indicating a coating degradation that leave a partially uncovered metal surface.

Those XPS results allows to argue that the three analysed samples behaves in a different way with the immersion in the aqueous solution, being the TG sample, without

Laponite nor cerium, the most susceptible one to undergo a detrimental damage. In the same way, the incorporation of Laponite, in TGL sample, carried to an improvement of the protective properties of the coating. On the other hand, if well the analysis of cerium is not easy to perform due to the XPS 3d spectra of cerium compounds present satellites peaks related to energy-gain (the so-called "shake-down" states) [24], it is clear that its incorporation, in sample TGL-Ce, produced the coating with the best performance in immersion. Table 3 shows the quantification the atomic compositions of the analysed samples obtained from its XPS surveys.

3.2. Electrochemical behaviour

Figure 5 shows anodic polarization curves of the coated system after 2h immersion in NaCl 0.35%m/v. It can be observed that all coated samples show a decrease in current density when compared with the bare alloy. Furthermore, clay nanoparticles containing coatings show even lower current density than the ones without clay nanoparticles. TGL and TGL-Ce coatings presented similar values of current density around corrosion potential but TGL show lower range of pseudopassivity compared with TGL-Ce. The reduction of anodic current density indicates that the anodic dissolution process of the steel is inhibited by the coating This can be associated to a reduction of the area available for the anodic and cathodic reactions for the presence of the film, since the electrochemical reaction take place in the defects [25]. Since TGLCe curve slopes change respect the bare substrate this can be and indicative that the silane barrier with cerium could act as a chemical barrier [26].

Figure 6 show the EIS results after 2h immersion in NaCl 0.35%m/v in the form of Bode plots where the effect of clay nanoparticles incorporation can be analysed. Clay nanoparticles containing coatings (TGL and TGL-Ce) show total impedance values more than one magnitude order higher than the ones without clay nanoparticles (TG) and even higher for

the bare steel (P). TG shows two time constants, one at high frequencies that can be associated to the coating and other at low frequencies related to the underneath corrosive process [21,27,28,29]. Conversely, the EIS response corresponding to the TGL and TGL-Ce coatings only depicts one time constant related to the coating evidencing a good barrier effect of the films. As the coating thickness for the three compositions are very similar, the reduction in the impedance modulus can be attributed to an area effect where clay nanoparticles are probably blocking the electrolyte access to the substrate.

Figure 7 shows the polarization curves after 24 h immersion in NaCl 0.35%m/v. It can be observed that TGL and TGL-Ce coatings present low values of current density, even lower than for 2 h of immersion for the TGL-Ce coatings. In opposition, coatings without clay nanoparticles show some kind of deterioration of the film since their response is very similar to the bare steel. The same effect can be seen in the EIS results (Figure 8). TG coatings present a drop in the phase angle and in the impedance modulus in the high region frequency when comparing with the 2 h immersion system, denoting the failure of the coating after immersion. Contrariwise, TGL-Ce coatings present a rise in the impedance modulus and phase angle comparing the same period of immersion. This behaviour is probably associated to the obstruction of defects due to cerium compound since this rise is not observed for the system without Ce.

To get a better insight of the coating performance, EIS data were fitted by mean of equivalent circuits using Zplot for Windows [18].

Model employed use Constant Phase Elements (CPE) instead of capacitances when phase angle was different from -90º. The impedance for the CPE, Z_{CPE}, element can be written as [30]:

$$Z_{CPE} = \frac{1}{Q(j\omega)^{\alpha}} \qquad (1)$$

where Q (pseudocapacitance) and α are the CPE parameters, independent of frequency, j is the current density and ω the frequency. As Q cannot represent the capacitance when $\alpha < 1$, it can be related with the effective capacity (C_{eff}) of the coating, applying a surface distribution of the elements [31]:

$$Ceff_{coat} = Q^{1/\alpha}\left(\frac{R_{sol}.R_{po}}{R_{sol}+R_{po}}\right)^{\frac{1-\alpha}{\alpha}} \qquad (2)$$

In the equation, R_{sol} is the solution or medium resistance and R_{po} is the resistance of the electrolyte in the coating pores. In the present work $Ceff_{coat}$ was calculated for the high frequency part of the impedance spectra, assuming a parallel array between the CPE of the coating and the R_{po} in the electric circuits [32]. Also, CPE_{dl} describes the inner layer between the bottom of the pores and the metal substrate. R_p is the polarization resistance in direct contact with the metal. Table 4 shows the electrical parameters values to the EIS results presented in Fig. 6 and 8 and C_{eff} calculation using eq 2. It is generally accepted the the pore resistance R_{po} is a measure of the porosity and degradation of the coating and the increase of coating capacitance $C_{effcoat}$ with time can be related to the water uptake into the film. Besides, the polarization resistance R_p, and double layer capacitance C_{efdl} can be related to the delamination of the coating and the presence of a corrosión phenomena [33].

It can be observed at the beginning of the immersion that TG, TGL and TGL-Ce present high resistance and low $C_{effcoat}$ of all the coating but there is a decrease in the resistance and an increase in the $C_{effcoat}$ of the coating for TG and TGL after immersion due to the developments of pathways in the silane film (Figure 9 a and b). These pathways are much developed for the coating without clay nanoparticles than for TGL evidencing the isolating features of the clays. At the bottom of the pores is where the corrosion issue takes place as it is evident from the value of C_{effdl} for the TG films together with a decrease in R_p resistance that can be associated with an increase in the exposed area (Figure 9 c and d). The increase in the in time of the

capacitance is observed for all the three coatings but in less degree for the TGLCe. This is probably due to the presence of hydrated cerium compounds precipitated in de defects, that increase the resistance but have different permittivity than the intact film. When comparing the effect of the cerium with the film without it, it can be observed that the presence of cerium in the coating enhance coating performance probably due to precipitation of cerium hydroxides as evidenced in the shift of the R_{po} parameter. This was previously observed by Naderi et al [34] in their work with sol-gel coating containing montmorillonite clay nanoparticles and cerium nitrate on aluminium and in our previous work [17].

The action of cerium in the film has been extensively studied onto many substrates. Hinton [35] suggested that cerium hydroxides precipitate on cathodic sites acting on the sites where oxygen reduction reaction takes place. Oxygen reduction releases hydroxyls ions and Ce(III) oxidizes to Ce (IV) precipitating as cerium hydroxide. Conversely, other authors affirm that act either as anodic, or mixed inhibitor [36,37,38]. The incorporation of silica nanoparticles in the silane containing cerium salts film can also improve corrosion resistance enhancing the crosslinking of the silane layer [9].

The results obtained in the present work show the films containing cerium in their composition present better anti-corrosion performance when compared with the ones without cerium. It is however important to note, that the presence of clay nanoparticles in the film strongly enhance the performance of the presented systems, since the corrosion resistance was significantly inferior for the coatings without clay nanoparticles.

4. Conclusions

A novel sol-gel material was synthesized with the incorporation of clay nanoparticles in order to improve the barrier properties and self-healing behaviour of cerium doped anticorrosive coatings. The incorporation of the laminar nanoparticles, up to 5 wt% in respect

to sol-gel silica network, improved considerably the physical integrity of the coating under immersion tests in 0.35 wt% NaCl water solution.

XPS analysis revealed that the addition of clay nanoparticles avoided the exposition of the metal substrate and the aparition of iron hydroxide, as a corrossion byproduct, after the immersion tests. Furthermore, with the incorporation of cerium and clay nanoparticles, only a small amount of Fe_2O_3 was observed after 24 h immersion at room temperature.

The electrochemical assays tests in 0.35 wt% NaCl water solution demonstrate that the incorporation of clay nanoparticles to the silane coating retard the diffusion of the electrolyte into the film when compared with the coating without clays. The incorporation of cerium salts shows the synergy between the clay nanoparticles and the cerium salt enhancing corrosion protection of the mild steel. Due to the known high adherence of sol gel coating this coating can act as prime coating offering both good wettability and retarding corrosion process.

Acknowledgements

The authors would like to thank the National Research Council of Argentina (CONICET, PIP 2012-0434) and to the National University of Mar del Plata (UNMdP, Project 15G/331) for the financial support.

References

[1] J.H. Osborne, K.Y. Blohowiak, S.R. Taylor, C. Hunter, G. Bierwagon, B. Carlson, D. Bernard, M.S. Donley, Testing and evaluation of nonchromated coating systems for aerospace applications, Progress in Organic Coatings 41 (2001) 217-225.

[2] W. Trabelsi, P. Cecilio, M.G.S. Ferreira, M.F. Montemor, Electrochemical assessment of the self-healing properties of Ce-doped silane solutions for the pre-treatment of galvanised steel substrates, Progress in Organic Coatings 54 (2005) 276-284.

[3] G.J.A.A. Soler-Illia, Molecular Chemistry of Sol–Gel Derived Nanomaterials. Edited by Robert J. P. Corriu and Nquyen Trong Anh, Angewandte Chemie International Edition 48 (2009) 8822-8823.

[4] G. Kickelbick, Introduction to Hybrid Materials, Hybrid Materials, Wiley-VCH Verlag GmbH & Co. KGaA, 2007, pp. 1-48.
[5] A. Conde, A. Durán, J.J. de Damborenea, Polymeric sol–gel coatings as protective layers of aluminium alloys, Progress in Organic Coatings 46 (2003) 288-296.
[6] S. Pellice, P. Galliano, Y. Castro, A. Duran, Hybrid sol-gel coatings produced from TEOS and γ-MPS, Journal of Sol-Gel Science and Technology 28 (2003) 81-86.
[7] A. Pepe, P. Galliano, M. Aparicio, A. Durán, S. Ceré, Sol-gel coatings on carbon steel: Electrochemical evaluation, Surface and Coatings Technology 200 (2006) 3486-3491.
[8] N.C. Rosero-Navarro, M. Curioni, R. Bingham, A. Durán, M. Aparicio, R.A. Cottis, G.E. Thompson, Electrochemical techniques for practical evaluation of corrosion inhibitor effectiveness. Performance of cerium nitrate as corrosion inhibitor for AA2024T3 alloy, Corrosion Science 52 (2010) 3356-3366.
[9] P.H. Suegama, H.G. de Melo, A.A.C. Recco, A.P. Tshiptschin, I.V. Aoki, Corrosion behavior of carbon steel protected with single and bi-layer of silane films filled with silica nanoparticles, Surface and Coatings technology 202 (2008) 2850 - 2858.
[10] J. Ballarre, D.A. López, W.H. Schreiner, A. Durán, S.M. Ceré, Protective hybrid sol-gel coatings containing bioactive particles on surgical grade stainless steel: Surface characterization, Appl Surf Sci 253 (2007) 7260-7264.
[11] M.G. Olivier, M. Fedel, V. Sciamanna, C. Vandermiers, C. Motte, M. Poelman, F. Deflorian, Study of the effect of nanoclay incorporation on the rheological properties and corrosion protection by a silane layer, Progress in Organic Coatings 72 (2011) 15-20.
[12] J.-M. Yeh, C.-L. Chen, Y.-C. Chen, C.-Y. Ma, K.-R. Lee, Y. Wei, S. Li, Enhancement of corrosion protection effect of poly(o-ethoxyaniline) via the formation of poly(o-ethoxyaniline)–clay nanocomposite materials, Polymer 43 (2002) 2729-2736.
[13] R. Herrera Alonso, L. Estevez, H. Lian, A. Kelarakis, E.P. Giannelis, Nafion–clay nanocomposite membranes: Morphology and properties, Polymer 50 (2009) 2402-2410.
[14] F. Deflorian, S. Rossi, M. Fedel, C. Motte, Electrochemical investigation of high-performance silane sol–gel films containing clay nanoparticles, Progress in Organic Coatings 69 (2010) 158-166.
[15] K.M. Seeni Meera, R. Murali Sankar, A. Murali, S.N. Jaisankar, A.B. Mandal, Sol–gel network silica/modified montmorillonite clay hybrid nanocomposites for hydrophobic surface coatings, Colloids and Surfaces B: Biointerfaces 90 (2012) 204-210.
[16] K. Joncoux-Chabrol, J.-P. Bonino, M. Gressier, M.-J. Menu, N. Pébère, Improvement of barrier properties of a hybrid sol–gel coating by incorporation of synthetic talc-like phyllosilicates for corrosion protection of a carbon steel, Surface and Coatings Technology 206 (2012) 2884-2891.
[17] I. Santana, A. Pepe, E. Jimenez-Pique, S. Pellice, I. Milošev, S. Ceré, Corrosion protection of carbon steel by silica-based hybrid coatings containing cerium salts: Effect of silica nanoparticle content, Surface and Coatings Technology 265 (2015) 106-116.
[18] Zplot for Windows, Electrochem. Impedance Software Operating Manual, Part 1 Scribner Ass. Inc. Southern Pines, NC (1998).
[19] K.J. Kubiak, M.C.T. Wilson, T.G. Mathia, P. Carval, Wettability versus roughness of engineering surfaces, Wear 271 (2011) 523-528.
[20] F. Moulder, W.F. Stickle, P.E. Sobol, K.D. Bomben, Handbook of X-Ray Photoelectron Spectroscopy, Physical Electronics, Inc. Eden Praire, Minnesota 55344, USA (1995).
[21] I. Milošev, Ž. Jovanović, J.B. Bajat, R. Jančić-Heinemann, V.B. Mišković-Stanković, Surface Analysis and Electrochemical Behavior of Aluminum Pretreated by

Vinyltriethoxysilane Films in Mild NaCl Solution, Journal of the Electrochemical Society 159 (2012) C303-C311.
[22] D. Arnott, N. Ryan, B. Hinton, B. Sexton, A. Hughes, Auger and XPS studies of cerium corrosion inhibition on 7075 aluminum alloy, Applications of Surface Science 22-23 (1985) 236-251.
[23] W. Trabelsi, E. Triki, L. Dhouibi, M.G.S. Ferreira, M.L. Zheludkevich, M.F. Montemor, The use of pre-treatments based on doped silane solutions for improved corrosion resistance of galvanised steel substrates, Surface and Coatings Technology 200 (2006) 4240-4250.
[24] I. Milosev, H.-H. Strehblow, The behavior of stainless steels in physiological solution containing complexing agent studied by X-ray photoelectron spectroscopy
Journal of biomedical materials research 52 (2000) 404 - 412.
[25] F. Andreatta, L. Paussa, P. Aldighieri, A. Lanzutti, D. Raps, L. Fedrizzi, Corrosion behaviour of sol–gel treated and painted AA2024 aluminium alloy, Progress in Organic Coatings 69 (2010) 133-142.
[26] D. Zhu, W.J. van Ooij, Corrosion protection of AA 2024-T3 by bis-[3-(triethoxysilyl) propyl]tetrasulfide in sodium chloride solution.Part 2: Mechanism for corrosion protection, Corrosion Science 45 (2003) 2177-2197.
[27] M.F. Montemor, A.M. Cabral, M.L. Zheludkevich, M.G.S. Ferreira, The corrosion resistance of hot dip galvanized steel pretreated with Bis-functional silanes modified with microsilica, Surf Coat Technol 200 (2006) 2875-2885.
[28] C. Liu, Q. Bi, A. Leyland, A. Matthews, An electrochemical impedance spectroscopy study of the corrosion behaviour of PVD coated steels in 0.5 N NaCl aqueous solution: Part II. EIS interpretation of corrosion behaviour, Corrosion Science 45 (2003) 1257 - 1273.
[29] F. Mansfeld, Use of electrochemical impedance spectroscopy for the study of corrosion protection by polymer coatings, Journal of applied electrochemistry 25 (1995) 187 - 202.
[30] C.H. Hsu, F. Mansfeld, Technical note: Concerning the conversion of the constant phase element parameter Y0 into a capacitance, Corrosion NACE 57 (2001) 747 - 748.
[31] B. Hirschorn, M.E. Orazem, B. Tribollet, V. Vivier, I. Frateur, M. Musiani, Determination of effective capacitance and film thickness from constant-phase-element parameters, Electrochimica Acta 55 (2010) 6218-6227.
[32] P.L. Bonora, F. Deflorian, L. Fedrizzi, Electrochemical impedance spectroscopy as a tool for investigating underpaint corrosion, Electrochimica acta 41 (1996) 1073 - 1082.
[33] N. Tang, W.J. van Ooij, G. Górecki, Comparative EIS study of pretreatment performance in coated metals, Progress in Organic Coatings 30 (1997) 255-263.
[34] R. Naderi, M. Fedel, F. Deflorian, M. Poelman, M. Olivier, Synergistic effect of clay nanoparticles and cerium component on the corrosion behavior of eco-friendly silane sol-gel layer applied on pure aluminum, Surface and Coatings Technology 224 (2013) 93-100.
[35] B.R.W. Hinton, J. Alloy Compd 15 (1992) 180.
[36] M.F. Montemor, A.M. Simões, M.G.S. Ferreira, Composition and behaviour of cerium films on galvanised steel, Progress in Organic Coatings 43 (2001) 274-281.
[37] M.F. Montemor, M.G.S. Ferreira, Analytical characterization of silane films modified with cerium activated nanoparticles and its relation with the corrosion protection of galvanised steel substrates, Progress in Organic Coatings 63 (2008) 330-337.
[38] M.F. Montemor, W. Trabelsi, M. Zheludevich, M.G.S. Ferreira, Modification of bis-silane solutions with rare-earth cations for improved corrosion protection of galvanized steel substrates, Progress in Organic Coatings 57 (2006) 67-77.

Legend to figures

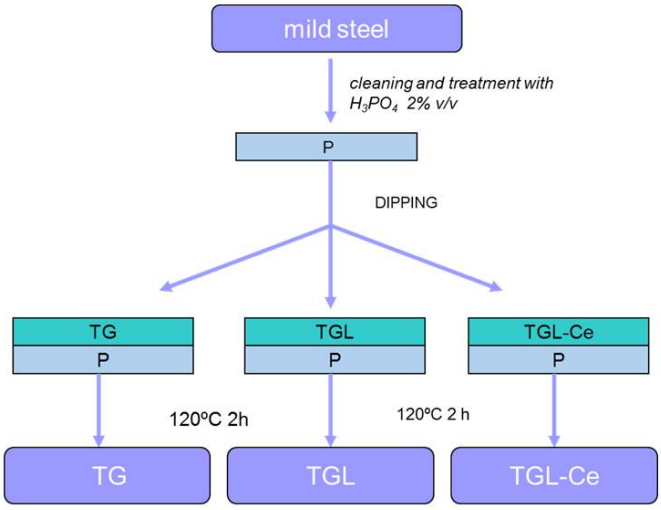

Figure 1. Schematic representation of samples preparation of TG, TGL and TGL-Ce coatings.

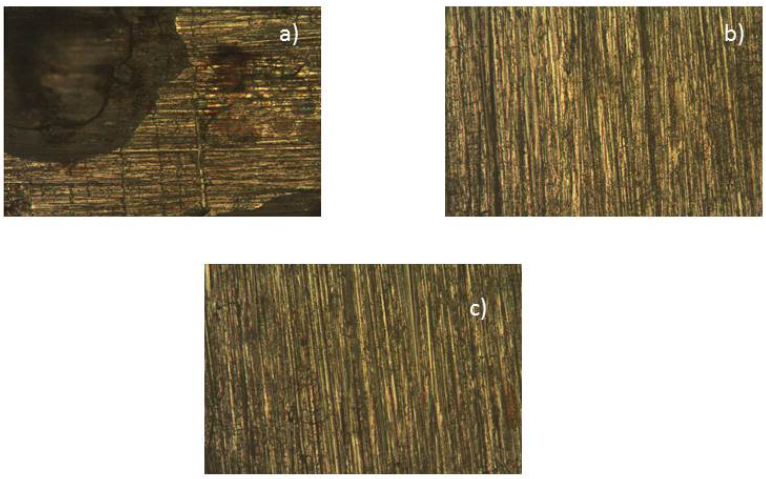

Figure 2. Optical microscopy, at 20x, of *a*) TG, *b*) TGL and *c*) TGL-Ce coated samples after 24 h immersion in 0.35 wt% NaCl water solution at room temperature.

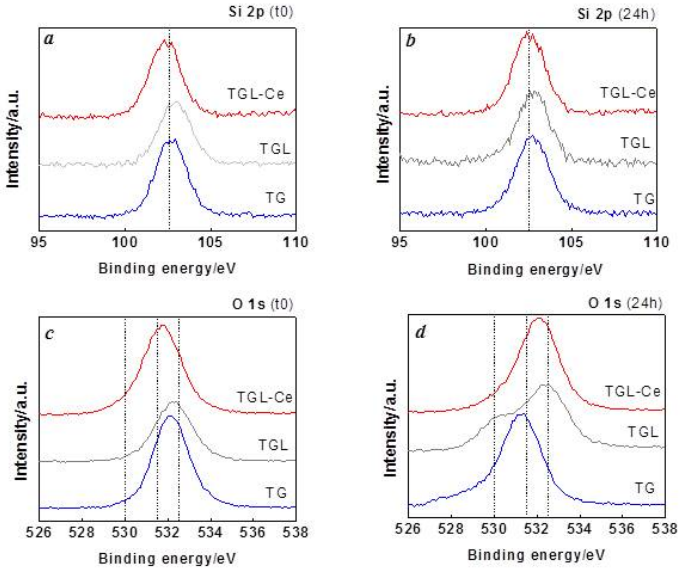

Figure 3. XPS high resolution spectra for mild steel samples with TG, TGL and TGL-Ce coatings for Si 2p, *a*) before and *b*) after 24 h immersion, and for O 1s, *c*) before and *d*) after 24 h immersion in 0.35 wt% NaCl water solution at room temperature.

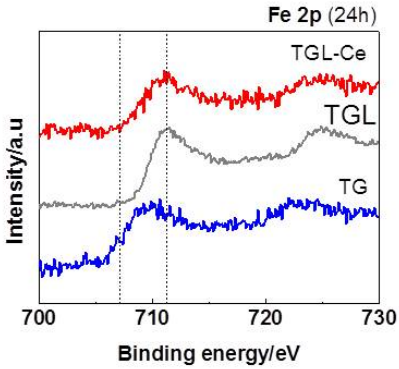

Figure 4. XPS high resolution Fe 2p spectra for mild steel samples with TG, TGL and TGL-Ce coatings after 24 h immersion in 0.35 wt% NaCl water solution at room temperature.

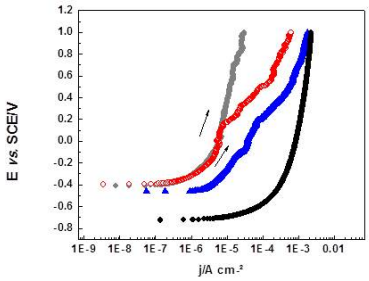

Figure 5. Anodic polarization curves for TG(▲), TGL(●), TGLCe(o) and P(●) after 2 h immersion in 0.35 wt% NaCl solution at room temperature.

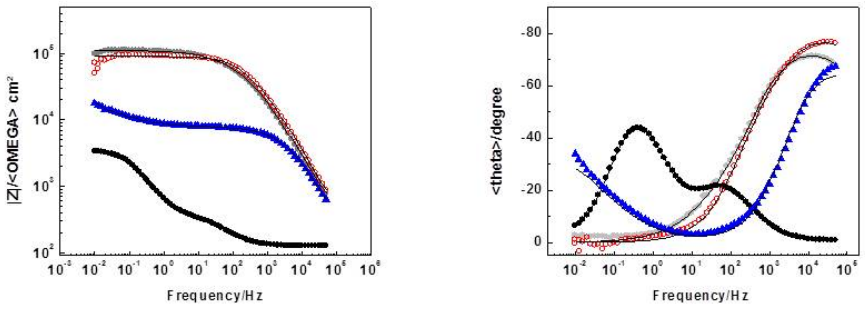

Figure 6. Bode plots for TG(▲), TGL(●), TGLCe(o) and P(●) after 2 h immersion in 0.35 wt% NaCl solution at room temperature. Solid lines represent the model fitting.

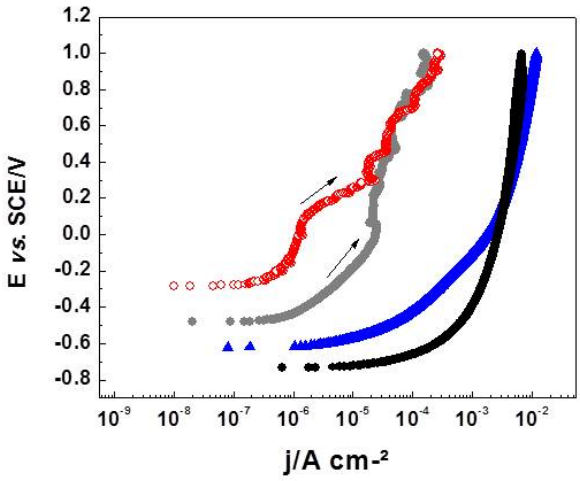

Figure 7. Anodic polarization curves for TG(▲), TGL(●), TGLCe(o) and P(●) after 24 h immersion in 0.35 wt% NaCl solution at room temperature.

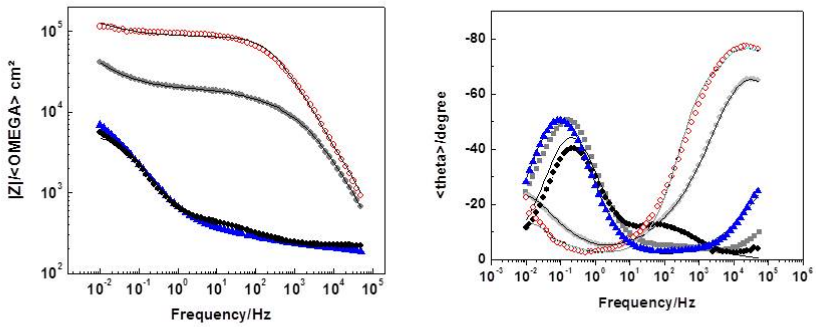

Figure 8. Bode plots for TG(▲), TGL(●), TGLCe(o) and P(●) after 24 h immersion in 0.35 wt% NaCl solution at room temperature. Solid lines represent the model fitting.

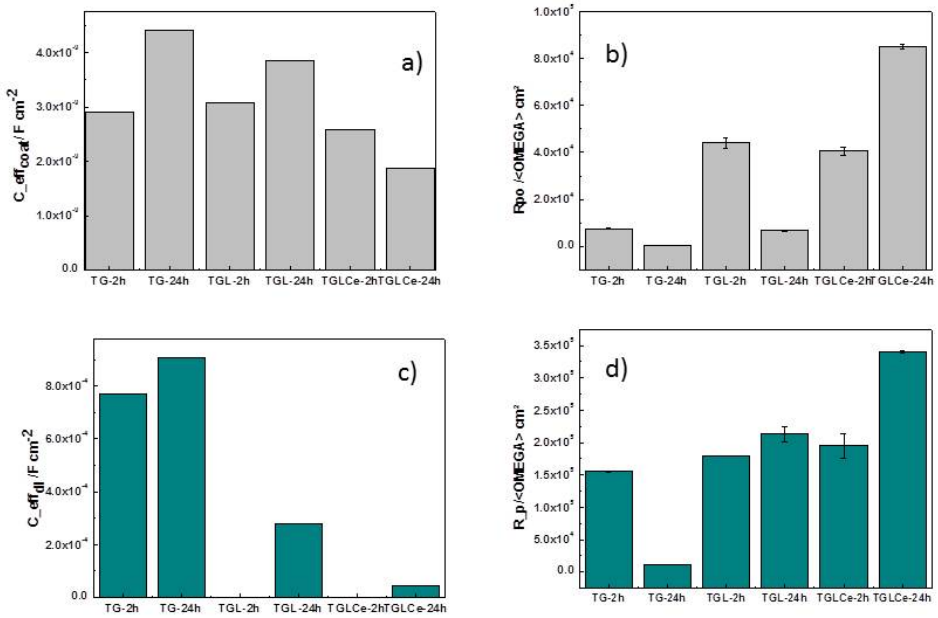

Figure 9. Variation of Ceff coat, Rpo, Ceffdl and Rp with immersion time (values from Table 4).

Table 1. Coating thicknesses of different compositions after thermal treatment.

Coating	**Thickness** (μm)
TG	2.00 ± 0.050
TGL	2.09 ± 0.195
TGL-Ce	2.21 ± 0.202

Table 2. Contact angle values of water drops at 20ºC.

Coating	**Contact angle** (º)
TG	69.7 ± 3.50
TGL	67.5 ± 2.05
TGL-Ce	70.3 ± 1.60

Table 3. Atomic compositions derived from the XPS survey spectra for TG, TGL and TGL-Ce samples before and after 24 h immersion in 0.35 wt% NaCl water solution at room temperature.

Sample		**% at**			
		Si	**O**	**Fe**	**Ce**
TGL-Ce	t_0	28.7	69.4	0.7	1.2
	24 h	24.5	71.8	3.7	-
TGL	t_0	30.2	69.5	0.3	-
	24 h	22.3	74.3	3.4	-
TG	t_0	31.1	66.2	2.7	-
	24 h	14.4	71.9	13.7	-

Table 4. Electrical parameters values corresponding to the EIS results presented in Fig. 6 and 8 and C_{eff} calculation using eq 2.

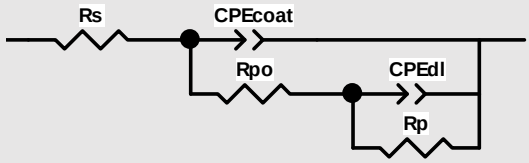

	R_{sol} (Ωcm^2)	Q_{coat} ($s\alpha\ \Omega^{-1}\ cm^{-2}$)	α_{coat}	R_{po} (Ωcm^2)	$Ceff_{coat}$ ($F\ cm^{-2}$)	Q_{dl} ($s\alpha\ \Omega^{-1}\ cm^{-2}$)	αdl	R_p (Ωcm^2)	$Ceff_{dl}$ ($F\ cm^{-2}$)
2 h immersion									
TG	50	$6.07\ 10^{-8} \pm 3.4\ 10^{-9}$	$0.8 \pm 4.9\ 10^{-3}$	$7.6\ 10^{3} \pm 51$	$2.91\ 10^{-9}$	$3.06\ 10^{-4} \pm 3.4\ 10^{-9}$	$0.53 \pm 1.9\ 10^{-3}$	$1.55\ 10^{5} \pm 5.1\ 10^{2}$	$7.7\ 10^{-4}$
TGL	50	$2.88\ 10^{-8} \pm 1.2\ 10^{-9}$	$0.85 \pm 3.6\ 10^{-3}$	$4.4\ 10^{4} \pm 3.2\ 10^{3}$	$3.08\ 10^{-9}$	$6.3\ 10^{-6} \pm 6.7\ 10^{-8}$	$0.53 \pm 2.6\ 10^{-3}$	$7.6\ 10^{4} \pm 302\ 10^{3}$	$3.31\ 10^{-6}$
TGLCe	50	$1.45\ 10^{-8} \pm 5.5\ 10^{-9}$	$0.89 \pm 7.4\ 10^{-3}$	$5.0710^{4} \pm 8.9\ 10^{2}$	$1.39\ 10^{-9}$	$1.38\ 10^{-7} \pm 47\ 10^{-8}$	0.67 ± 0.01	$5.04\ 10^{5} \pm 1.9\ 10^{4}$	$3.31\ 10^{-6}$
24 h immersion									
TG	50	$4.5610^{-6} \pm 4.7\ 10^{-7}$	$0.55 \pm 2.4\ 10^{-3}$	$5.510^{2} \pm 31$	$4.41\ 10^{-9}$	$6.7\ 10^{-4} \pm 6.7\ 10^{-5}$	$0.79 \pm 1.1\ 10^{-3}$	$1.06\ 10^{4} \pm 1.10^{2}$	$9.16\ 10^{-4}$
TGL	50	$2.610^{-8} \pm 8.2\ 10^{-10}$	$0.87 \pm 2.4\ 10^{-3}$	$6.8\ 10^{3} \pm 242$	$3.84\ 10^{-9}$	$1.8\ 10^{-4} \pm 8.7\ 10^{-6}$	0.55 ± 0.02	$2.13\ 10^{5} \pm 1.2\ 10^{3}$	$2.81\ 10^{-4}$
TGLCe	50	$2.510^{-8} \pm 1.3\ 10^{-9}$	$0.84 \pm 5\ 10^{-3}$	$8.5\ 10^{4} \pm 1.2\ 10^{3}$	1.8710^{-9}	$6.87\ 10^{-5} \pm 8.07\ 10^{-6}$	0.46 ± 0.04	$3.40\ 10^{5} \pm 1.2\ 10^{3}$	$4.27\ 10^{-5}$